BELT DRYING OF SUPPORTED CATALYSTS

By

HAO CHEN

A thesis submitted to the

Graduate School – New Brunswick

Rutgers, The State University of New Jersey

In partial fulfillment of the requirement

For the degree of

Master of Science

Graduate Program in Chemical and Biochemical Engineering

Written under the direction of

Benjamin J. Glasser

And approved by

_____

_____

_____

New Brunswick, New Jersey

May, 2015

ABSTRACT OF THE THESIS

Belt Drying of Supported Catalysts

By HAO CHEN

Thesis Director:

Dr. Benjamin J. Glasser

Supported catalysts are widely used in the chemical industry due to their (1) high surface area, (2) decreased requirement of expensive active components and (3) high mechanical and thermal stability. Many factories use belt conveyors to dry the supported catalysts after the impregnation. Although the belt drying technology has been developed for many years, the method of controlling the product is mainly trial and error. This can potentially waste a lot of energy and materials when optimizing the product quality. Therefore, it is important to study the behavior of the drying process and its effect on product characteristics. In this thesis, a novel method is introduced using a packed bed dryer to mimic the belt drying process. A Nickel/Alumina catalyst was studied in both one-heating zone and multi-heating zone systems. BET and micro-XRF were used to measure the catalyst pore structure and the metal distribution after drying, respectively. A pronounced egg-shell metal distribution was found in the one-heating zone system. Moderate egg-shell metal distributions were found in two-heating zone system due to the effect of melting point depression and film breakage during the drying process.

Acknowledgement

I would like to express the deepest appreciation for my advisor, Professor Benjamin J. Glasser, who has given me suggestions and patient instructions on this thesis. Without his guidance and persistent help, this thesis would not have been possible. I would like to thank my co-advisor, Professor Xue Liu, who is kind and patient with his students. During the last year, Professor Liu has guided me through all the experimental parts of this thesis. Also, I wish to express my sincere gratitude to Professor Gene Hall and Dr. Arya Tewatia for their help on the micro-XRF and DSC analyses. I wish to thank Cody Bishop for the suggestions on this thesis. I also thank Si Chen, Sathish Kumar Gajula, Thamer A. Omar and all the group members who have helped make wonderful memories during the work. I thank Saint-Gobain Norpro Corporation for their generous donation of the materials. I also thank the Rutgers Library of Science and Medicine for their assistance in finding literature. And lastly, the people who made these two years at Rutgers a wonderful experience: Wenqi Ding, Tianrui Li, Ting Li and Jonathan Pai. Thank you all for the valuable memories.

Contents

Chapter 1

Introduction

Supported catalysts are widely used in a variety of industrial application due to their large specific surface area, low requirements of precious metal precursor and high thermal and mechanical stability.[1,2] Supported catalysts usually consist of an active component, either a base metals (e.g. Ni, Ba) or precious metals (e.g. Pt, Au), and a porous supporting materials (e.g. silica, alumina). With respect to the distribution of metal precursors, four main categories can be distinguished: uniform, egg-shell, egg-white and egg-yolk.[3,4] Figure 1 shows four typical types of metal distribution. The environment of the reactor and the required reaction rate are usually taken into consideration when determining the metal distribution profile. For example, (d) egg-yolk (catalyst concentrated at the central layer) and (c) egg-white (catalyst concentrated at the middle layer) distributions are usually adopted in fluidized or moving bed reactor where intense abrasion and attrition occurs between the particles.[5] (b) Egg-shell (catalyst concentrated in the external layer) distribution is suitable for reactions that are mass transfer limited. (a) Uniform distributions are advantageous for slow reactions.

Figure 1. Four main types of catalyst profile.

The preparation of supported catalysts typically involves three steps: impregnation, drying and calcination.[6] Impregnation is a process in which the active metal component is deposited on or into the catalyst support. [7] A lot of research has been focused on the impregnation process due to its significant impact on the distribution of metal precursor.[8-11] Depending on the amount of aqueous solution used, two types of impregnation can be distinguished: dry impregnation and wet impregnation. Dry impregnation, also called "incipient wet impregnation" or "IWI", occurs when the amount of the solution used for impregnation is less than or comparable to the pore volume in the support material.[8] This method is suitable for impregnation with precious metals due to the high utilization efficiency. However, in wet, or "soaking", impregnation, the catalyst carriers are immersed in a large amount of solution with high metal ion concentration. Therefore, supported catalysts with cheap base metal are usually prepared in this way. Several studies have shown that impregnation and drying of one metal component can only lead to uniform, egg-shell and egg-yolk distributions. [2,10]. If another metal component is introduced during impregnation, a moderately egg-yolk profile can be obtained due to the interaction between different ions. Additionally, a shift from egg-white to egg-yolk profile can be observed with increasing impregnation time. [3] One experiment showed that, for a supported catalyst of Pt/γ-Al_2O_3, 1-hour impregnation leads to an egg-white profile, and 22-hour impregnation leads to an egg-yolk profile.[4]

The drying process is usually carried out after the impregnation to remove the liquid solution from the support. Three stages can be observed during the drying process: the preheating period, the constant-rate period and the falling-rate period.[9,10] At the beginning

of the drying process, in the pre-heating period, the bulk wet material increases in temperature. During the constant-rate drying period, the liquid solution moves toward the external surface of the support, driven primarily by capillary force, while metal components are transported by diffusion.[12] The drying rate is controlled by the external conditions including the drying gas temperature and flow rate , the total pressure in the environment and the partial vapor pressure of the solution.[13] At the end of the drying process, the falling rate period, the external solution has evaporated and the drying rate drops dramatically with time. This period can be observed when the internal mass transfer rate dominates the process and the surface pressure of the materials is decreasing with the drop of moisture content.

The distribution profile is commonly believed to be controlled by the impregnation process and therefore the effects of drying can usually be ignored. The metal complex will redistribute if the adsorption between the support and metal component is weak. Due to the complexity of such a mechanism, only a few theoretical models have been introduced. Waananena et al. summarized the drying mechanisms in a review paper in 1993 and provided the classification of drying process.[13] Neimark's group was one of the first to develop a theoretical model for the drying process.[6,14] They have defined slow drying and fast drying regimes using a dimensionless number. According to their theory, the egg-shell profile is more favorable at slow drying rate while a relatively high drying rate results in a uniform metal distribution. This agrees with the results from the work of Komiyama et al.[15] Komiyama proposed a "reservoir" model to explain this phenomenon. In this model, the porous structure is described as a support with a few macro-pores and lots of micro-pores. Due to capillary pressure, the liquid solution is drawn from the macro-pores to the micro-

pores, which works as a “reservoir”. When the heating rate is relatively slow, the metal precursors are sucked towards the external surface and the egg-shell profile is formed. At higher drying rates, however, the interconnection between macro- and micro-pores is relatively weak and the metals are deposited in the same location as after impregnation.

A more detailed model was provided by Lee et al. and Uemura et al.[2,16] Uemura extended the “reservoir” model and developed a quantitative calculation. Lee established models based on capillary flow and metal diffusion to describe the redistribution of metal precursors during the constant-rate drying period. However, they didn’t take into account the processing parameters and the material properties. A more recent work by Lekhal et al. used a dusty gas model and Darcy’s law to describe the gas and liquid phase, respectively. [3,10,17] Transport of metal components are modeled by the Nernst-Planks equation. In addition, a Langmuir model was applied to describe the adsorption and desorption for the metal redistribution during the drying.

Recently, some studies have focused on applying these models to belt conveyors with multiple heating zones, which are commonly used in the food and chemical industries.[18-20] Advantages of belt drying includes: 1) a simple geometry that allows steady operation, 2) uniform drying due to the movement of product, 3) a multi stage belt systems that can be adjusted for different drying requirements and 4) use in a continuous systems. Xue et al. developed a layering model to simulate the packed bed drying process.[18] At the beginning of the drying process, where an equilibrium state is reached between the wet samples and the humid drying air, the upper layer of the materials have not yet started to dry. As the drying process continues, the equilibrium breaks when the humidity in the drying air decreases to a certain point and water evaporation starts in the upper layer. Although the

constant-rate period drying profile may differ for different layers, they share a similar falling-rate stage. As a result, the metal distribution is similar in different layers indicating that the falling-rate period dominates the metal distribution profile.

In this thesis, multi-heating zone systems are studied using different metal precursors to verify the previous model developed by Xue et al. The effect of drying using two heating zones in a packed bed system on the distribution of high and low metal precursors is studied to obtain a deeper understanding of the mechanism of belt drying processes. The rest of the thesis is organized as follows. In Chapter 2 results for drying of a supported catalyst are presented and discussed. In Chapter 3 conclusions and future work are presented.

Chapter 2

2.1. Method

2.1.1 Mimicking a Belt Dryer Using a Packed Bed

Belt drying is a well-developed technology in the food and chemical industries. When supported catalysts are dried, two of the most important parameters are the temperature profile and the humidity profile along the belt. Some of the catalysts are temperature sensitive, where the metal distribution could potentially be very different when heated even slightly above the melting temperature of the metal. Therefore investigating the temperature profile is the first and foremost task in this study. We used the packed bag drying process to mimic the procedure of belt drying. Figure 2 and figure 3 provide a simple illustration of how this happens.

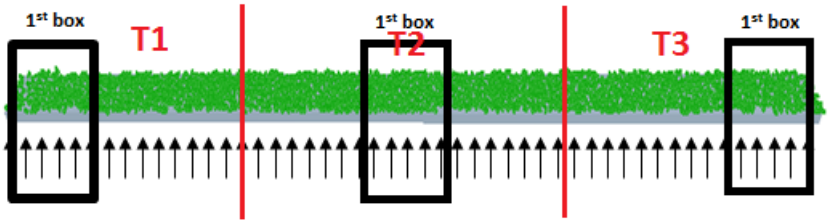

Figure 2. A typical belt dryer with three heating zones

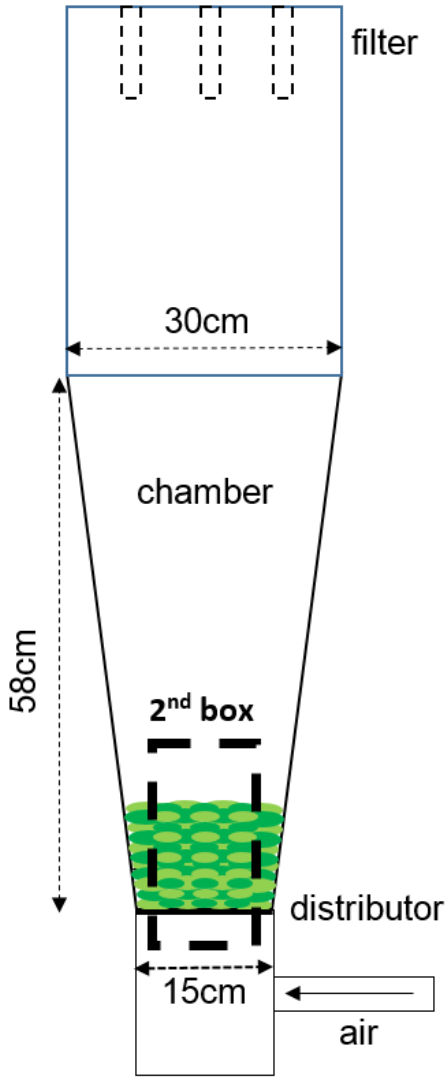

Figure 3. A schematic figure of catalyst drying using Glatt GPCG-1 fluidized bed dryer.

A schematic figure of a typical belt conveyor is shown in figure 2. Supported catalysts are evenly distributed on the belt,which transports the pellets at a constant rate from the left to the right. The heating air flows up from the bottom and removes moisture from the wet materials. The belt dryer is usually divided into several heating zones as shown in the figure. The heating temperature can be adjusted in each heating zone to obtain different temperature profiles. Some food enterprises require a temperature switch of high-to-low

for special food flavor. A low-to-high temperature profile usually leads to a relatively gentle heating process. In figure 3, the supported catalysts are placed in a Glatt GPCG-1 fluidized bed dryer. The heating gas flows from the bottom and passes through the distributor. In order to prevent the catalysts from being fluidized, the gas flow rate is carefully controlled at a low level. As we track the materials inside the 1st box in figure 2, the temperature profile and the properties of these catalysts (i.e. metal profile) are changing as a function of location on the belt. In the 2nd box of figure 3, the temperature and the properties of the catalysts change with time. Therefore, we expect to obtain similar profiles of temperature and metal distribution in the 1st and the 2nd box. There are some differences between the belt and the packed bed. One major difference is the heat losses at the walls of the packed bed. However if these heat losses are relatively small then the two systems can potentially be quite similar.

2.1.2 Drying Mechanism

The catalyst we have used in this study is nickel ions supported on the cylindrical alumina pellets. The alumina pellets were immersed in the nickel nitrate solution and were then put into the dryer. The drying mechanism of these porous pellets was studied by Xue et al.[1,18,21]

During the drying process, several phenomena are taking places simultaneously inside the porous structure as shown in figure 4: (1) solvent (water) evaporation into the heating gas; (2) the motion of dissolved metal due to capillary flow, back-diffusion and the receding drying front; (3) adsorption and desorption of the metals.

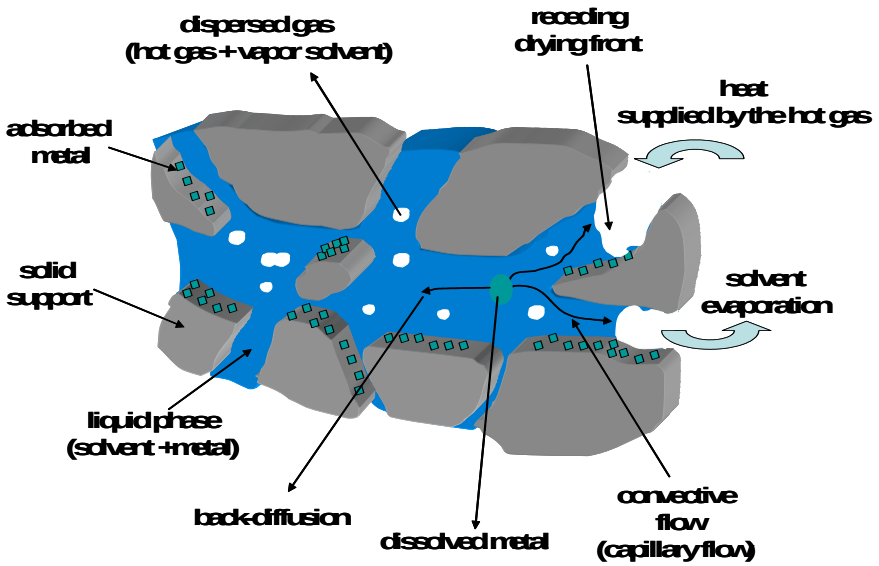

Figure 4. Courtesy of B. Glasser, X. Liu and J. Khinast. Schematic figure of drying mechanism in alumina pellets

The complex system was decoded by establishing a series of mass and energy transfer equations between the gas phase (heating air, solvent vapor) and the liquid phase (solvent and the metal precursor). The following equations describe the drying process.[21]

$$\frac{\partial}{\partial t}\left(\varepsilon_g C_{g,a}\right) = -\frac{1}{r}\frac{\partial}{\partial r}\left(rN_{g,a}\right) \tag{1}$$

$$\frac{\partial}{\partial t}\left(\varepsilon_l C_{l,a} + \varepsilon_g C_{g,s}\right) = -\frac{1}{r}\frac{\partial}{\partial r}\left(\alpha r N_{l,s} + rN_{g,v}\right) \tag{2}$$

$$\frac{\partial}{\partial t}\left(\varepsilon_l C_{l,i}\right) = -\frac{1}{r}\frac{\partial}{\partial r}\left(\alpha r N_{l,i}\right) - \rho_s R_i \tag{3}$$

$$\frac{\partial}{\partial t}\left(C_{s,i}\right) = R_i, \qquad i = metal\ component \tag{4}$$

$$\frac{\partial}{\partial t}\left(\sum_{i=1}^{2} \varepsilon_g C_{g,i} h_{g,i} + \varepsilon_l C_{l,i} h_{l,i} + \rho_s h_s\right) == -\frac{1}{r}\frac{\partial}{\partial r}\left(\sum_{i=1}^{2} rN_{g,i} h_i + \alpha r N_{l,s} h_l - r\lambda \frac{\partial T}{\partial r}\right) \tag{5}$$

$C_{g,a}$ and $C_{g,s}$ are the concentration of the heating air and the solvent vapor in the gas phase, respectively. $C_{l,s}$ and $C_{l,i}$ are the concentration of solvent and the dissolved metal in the liquid phase, respectively. $C_{s,i}$ is the concentration of metal adsorbed on the support. Similarly, $N_{g,a}$, $N_{g,v}$, $N_{l,s}$ and $N_{l,i}$ are the fluxes of the air, the solvent vapor, the solvent and the dissolved metal, respectively. ε_g and ε_l are the volume fractions of the gas and liquid phases. ρ_s represents the density of the alumina pellets. R_i represents the rate of metal adsorption. $h_{g,i}$ represents the enthalpy of the solvent or the air. h_l and h_s are the enthalpy of the liquid and solid. λ is the effective thermal conductivity. α is the film-breakage factor that related to the liquid fraction. Equations (1) and (2) describe the mass balance of heating gas and solvent in the supported pellets. Equations (3) and (4) represents the mass balance of the adsorption and desorption of the dissolved metal. Equation (5) describes the energy balance.

2.2. Materials and Experiment Setup

2.2.1 Materials

The Nickel/Alumina system was studied in this work. Cylindrical ϒ-alumina pellets (Saint-Gobain Norpro, Stow, OH, USA) were used as solid supports. As shown in figure 5, these pellets are 3 mm in diameter and approximately 10 mm in length. Almina is a porous material that is commonly adopted as solid support in chemical industry. It has relatively high surface area. According to BET analysis, the average surface area of the pellets used in this study is 238 m^2/g. The thermal property of the alumina pellets is also very stable, as the melting point is around 2072 °C. The pore size distribution of the alumina pellets will be shown and discussed in a later part of this thesis. Nickel nitrate hexahydrate powders (Sigma-Aldrich, St. Louis, MO, USA) were used as metal precursors.

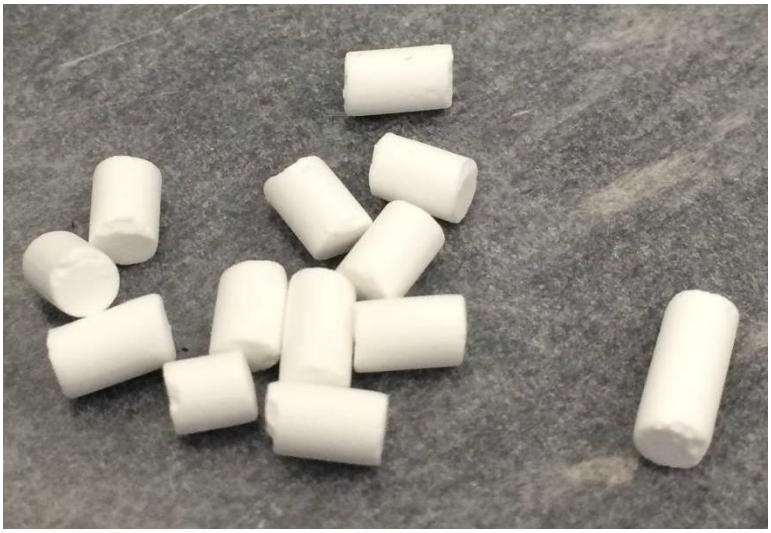

Figure 5. SA 6176 3mm alumina pellets

When heating up to around 60 °C, the nickel compound starts to lose bound water and melts in the porous structure. After all of the bound water evaporates, the melting point of the nickel can increase significantly.

2.2.2 Experiment Setup

2.2.2.1 Pellet Preparation

The alumina pellets were pre-treated to ensure the consistency in all batches. SA 6176 3mm alumina pellets (230 g) were firstly preheated in an oven at 120 °C for 12 hours to remove the moisture inside the porous structure. As shown in figure 6, the dried pellets were then immersed into 700 ml of 1M $Ni(NO_3)_2$ solution immediately for impregnation. The whole impregnation process took 5 days to allow the system to reach the equilibrium state (i.e. the adsorption rate of the dissolved metal equals the desorption rate).

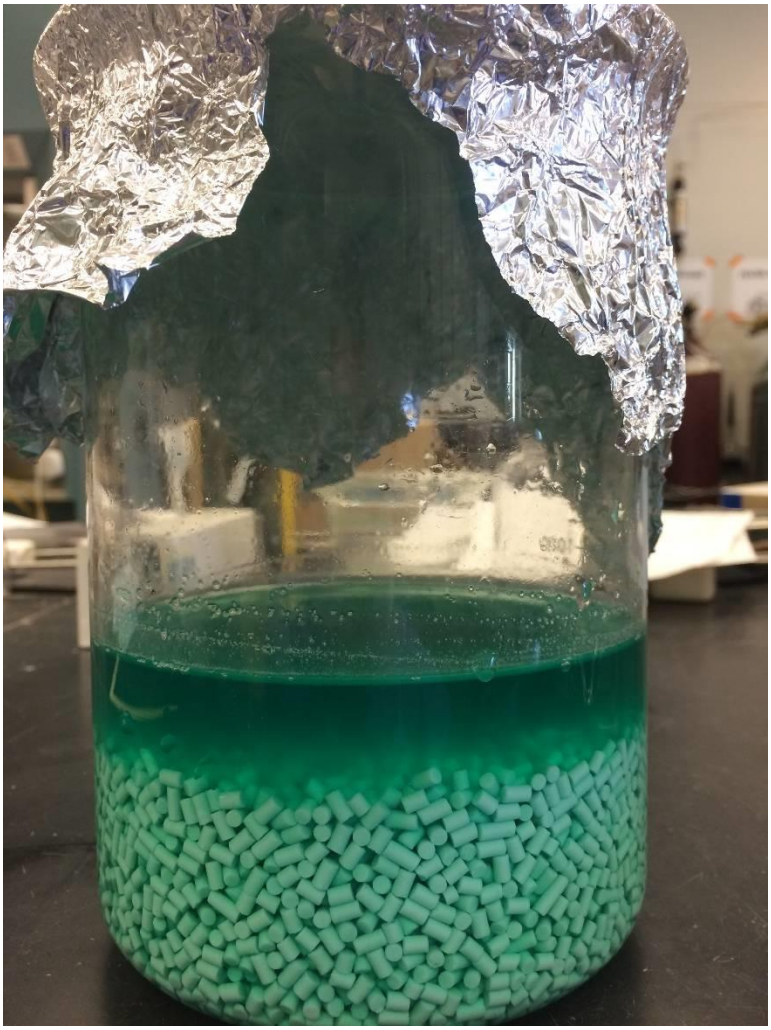

Figure 6. Impregnation of SA 6176 3mm alumina pellets in 1M $Ni(NO_3)_2$ solution.

2.2.2.2 Drying Procedures

The drying process was performed in a Glatt GPCG-1 fluidized bed dryer (Glatt, Binzen, Germany). Figure 3 shows the geometry size of the dryer. An air distributor (15 cm in diameter) was placed at the bottom of the chamber to support the catalysts. The depth of the catalyst bed was 2.54 cm. Three temperature probes were plugged into the top, the

middle and the bottom layer of the bed to evaluate the temperature profile of different positions. The dryer was equipped with a compressor and a desiccant air dryer (VAN AIR, Michigan City, IN, USA) that provided a constant inlet airflow of 1.2 m/s, ensuring sufficient driving force for drying without fluidizing the bed. For the one-heating zone study, the drying temperature was set at 100 °C. For the two-heating zones study, two heating patterns were adopted: (1) preheated at 60 °C for 10 minutes and then switched to 150 °C until the end and (2) preheated at 150 °C for 10 minutes and then switched to 60 °C until the end. A humidity monitor was placed at the exhaust air to determine the end-point of the drying process.

2.2.2.3 Pellet Characterization

The pore size distribution and the specific surface area were evaluated via TriStar 3000 gas adsorption analyzer (Micromeritics Instrument Corporation, Norcross, GA, USA) with nitrogen as the analytical gas. Brunauer-Emmett-Teller (BET) adsorption method was used to evaluate the specific surface area over a range of relative pressures (between 0.05 and 0.3). Brunauer-Joyner-Halenda (BJH) adsorption and desorption method was employed to determine the pore size distribution. Prior to analysis, approximately 100 mg of the alumina pellets were weighed and degassed at 100 °C with nitrogen for 12 hours to remove moisture. The gas adsorption and desorption occurred at the temperature of liquid nitrogen (i.e. -196 °C).

To investigate the metal profiles after drying, the catalyst samples were cut in half in the radial direction and the radial nickel profile was measured using micro-X-ray fluorescence spectroscopy (XRF). The Ni/Alumina ratio was used to report the metal concentration at a given position R/D, providing an evaluation of the metal profile.

The melting behavior of nickel nitrate hexahydrate in the alumina pellets was investigated via differential scanning calorimetry (DSC) measurements performed with DSC Q1000 (TA Instruments, New Castle, DE, USA). The experiment was performed according to the procedure in T. M. Eggenhuisen et al.[22]. The pellet samples were cut into four pieces, each weighing approximately 10 mg. The measurement followed a heat-cool-heat pattern of 80 °C, -75 °C and 80 °C, respectively, at 2.5 °C/min with 5 min isothermal steps at each temperature extreme. The thermograms of the samples were obtained using Universal Analysis 2000 (TA Instruments, New Castle, DE, USA).

2.3 Results

2.3.1 Temperature Profile

In general, the redistribution of the metal precursor in supported catalysts is characterized by the heating conditions during the drying process. The supported catalysts tend to form an egg-shell distribution with mild drying conditions where the drying rate is slow. Uniform distribution is favored during intense heating due to the back diffusion at the end of the drying process.

In each heating zone of the belt conveyor drying system, where the heated air temperature was kept at a constant level, the materials at the bottom layer heated up first, followed by those in the top layer. Similarly, in packed bed drying system, the heated air flows through from the bottom to the top, thus the temperature at the bottom layer increases first. Figure 7 shows the temperature profile in the top and bottom layers of the particle bed when applied with heated air at (a) 60 °C and (b) 100 °C. For both operating conditions, similar behaviors were observed: (1) the temperature at the bottom layer increased immediately after the drying process had begun and (2) the top part of the particle bed endured an

obvious preheating period before the temperature started to increase. It can be concluded that the upper layers experienced a milder drying process than the lower layers in the particle bed. Additionally, for higher heating temperature, as shown in figure 7, the increase in temperature is more rapid, indicating a more intense drying pattern.

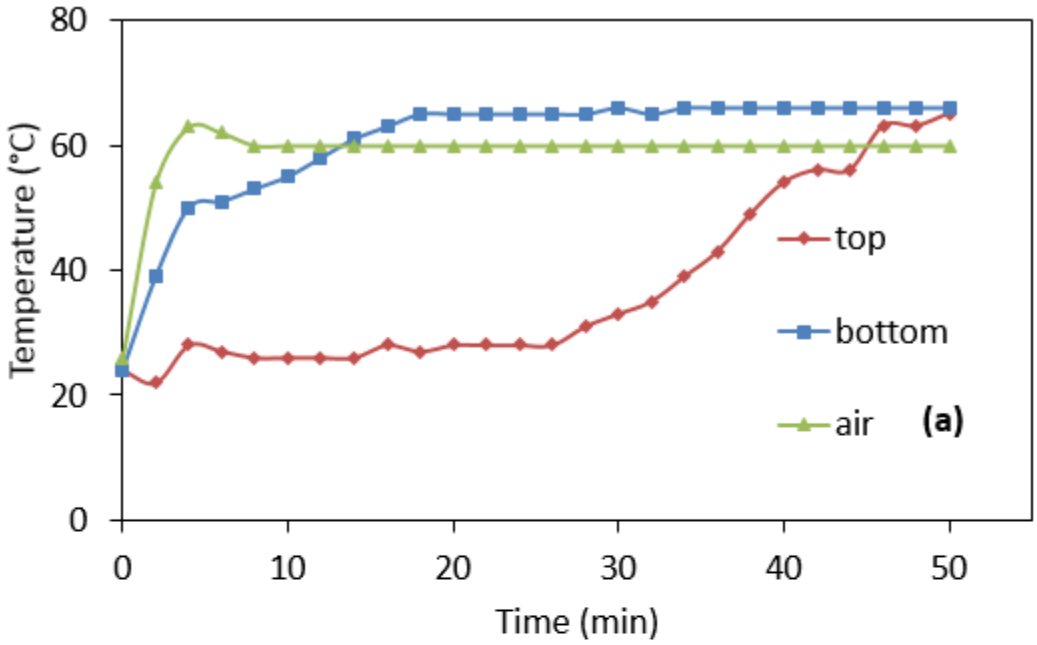

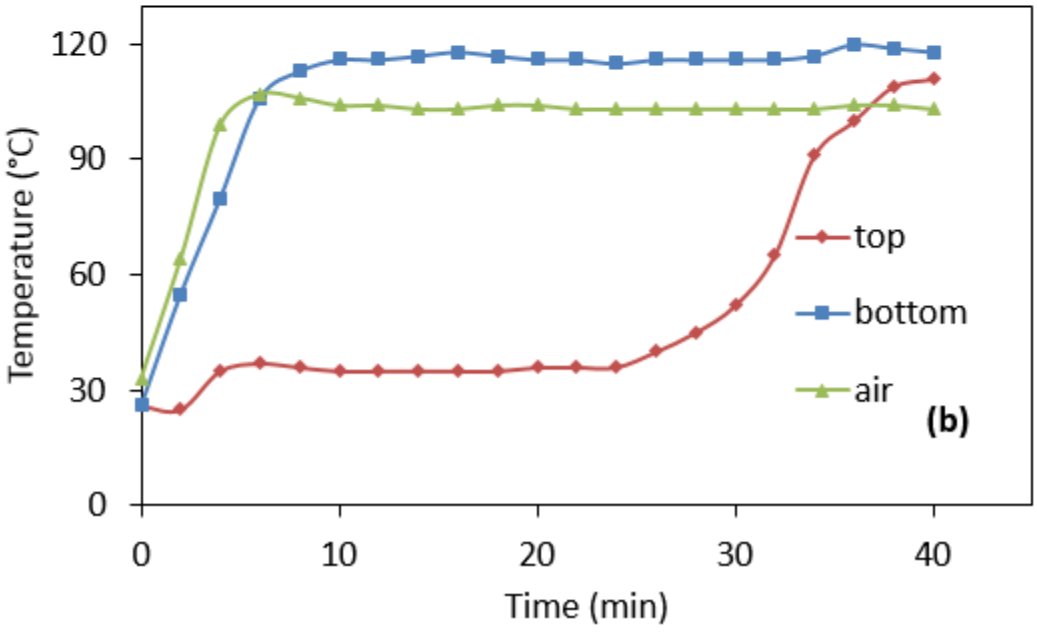

Figure 7. Temperature profile for catalyst at different positions of the chamber. (a) Drying at T = 60 °C, heating air flow rate v = 1.2 m/s; (b) Drying at T = 100 °C, heating air flow rate v = 1.2 m/s

The situation becomes more complicated when the temperature switch is introduced in multi-heating zone systems. In the study of the two-heating zone system, two switch strategies were investigated. Figure 8 shows the temperature profiles obtained from the low-to-high and the high-to-low switch drying process. In each case, similar to the one-heating zone situation, the temperature increased immediately at the bottom layers, and the upper layers had a warm-up period before the temperature increased. Furthermore, the warm-up period is increased with the increasing height in the particle bed. Due to the delay in heat transfer, as compared to the single drying method in one-heating zone systems, the temperature profile for upper layers can be decoupled from the bottom lower layers in some extreme cases. In figure 8 (b), the heating air temperature switched from 115 °C to 60 °C at 10 min. The bottom layer reached the peak almost the same time when heating air raised up to 115 °C. However, the middle layer has only reached about 90 °C and the bottom layer has yet just started to warm up. The different temperature profiles between the layers can affect the resulting metal distribution, especially when the switch point is near the melting point of the loaded metal compounds. It can be expected that the metal distribution is not similar among the different layers, which might be a concern for drying supported catalysts on a belt conveyor dryer with several heating zones.

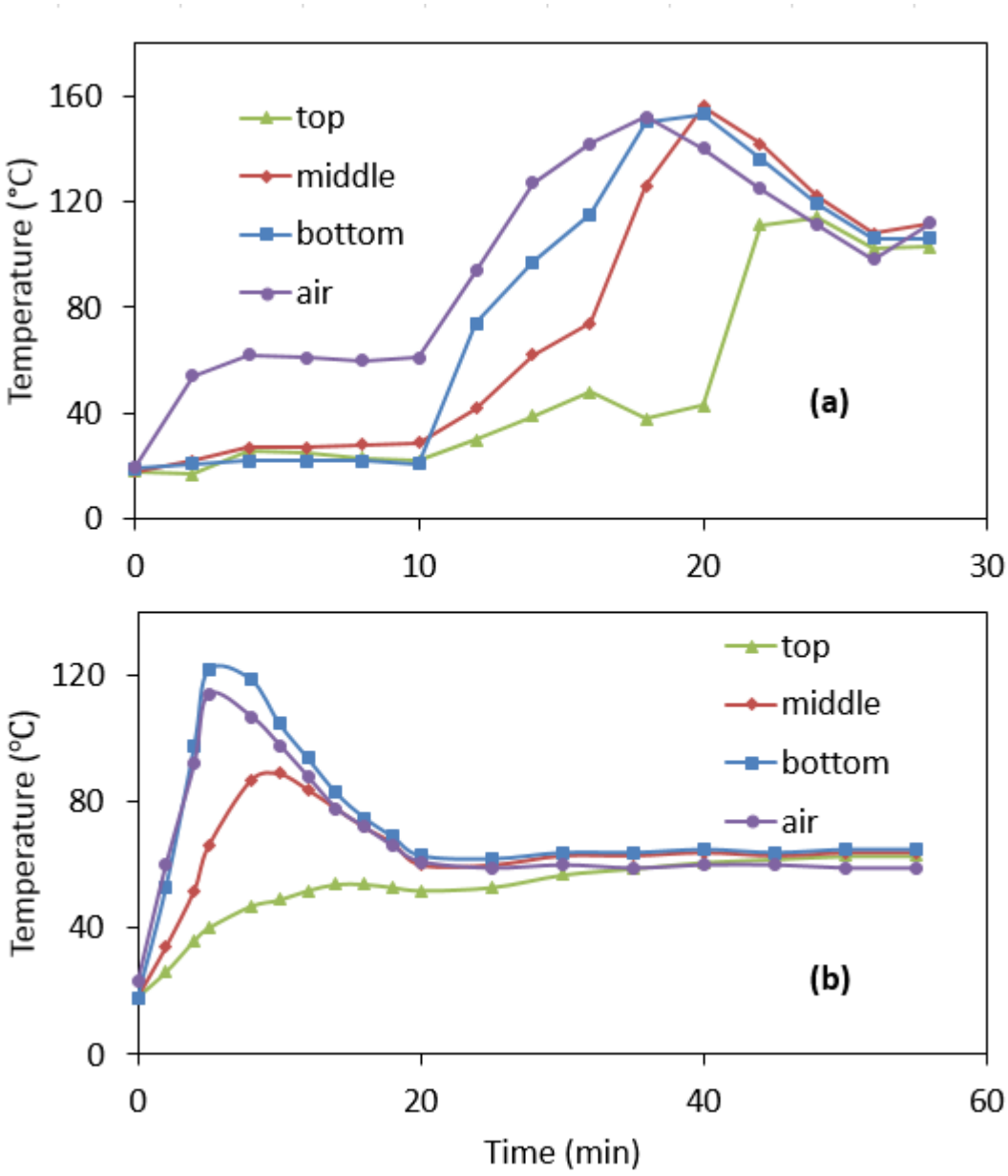

Figure 8. Temperature profile for the catalysts (impregnated in 1M $Ni(NO_3)_2$ solution) using two-heating zone drying method: (a) Drying at T_1 = 60 °C then T_2 = 150 °C; (b) Drying at T_1 = 115 °C then T_2 = 60 °C

2.3.2 BET Surface Area and BJH Pore Size Distribution

The characterization of the pore structure inside the supported catalysts was studied via nitrogen adsorption analysis. Figure 9 and figure 10 show the pore size distribution and the

nitrogen adsorption isotherm of the supporting materials before and after loading with the metal. The peaks of the pore distribution curves indicate the average pore size is 9.4 nm for both samples. However, the pore volume at the peak drops from 2.1 cm^3/g to 1.1 cm^3/g due to the metal loading.[23] As can be observed from the figures, a drop in pore volume appears in almost all range of pore width, which indicates that there is no pore size preference for the metal adsorption. The nitrogen adsorption isotherm (inset) can help explain the meso-pore structure of the materials.[24,25] Type IV isotherm and a combination of HI and H4 hysteresis loop type were both observed from both samples at relative pressure ranging from 0.7 - 1.0, which reveals the branch-like pore structure of the pellets. The meso-scale cylindrical pore channels are surrounded by the narrow slit pores including pores in the micro-pore region. Moreover, it was confirmed from the isotherm data that all materials retained their meso-porosity even after metal loading. [23] The surface area dropped from 232.99 m^2/g to 172.79 m^2/g, which can be considered as an indication of a successful metal loading.

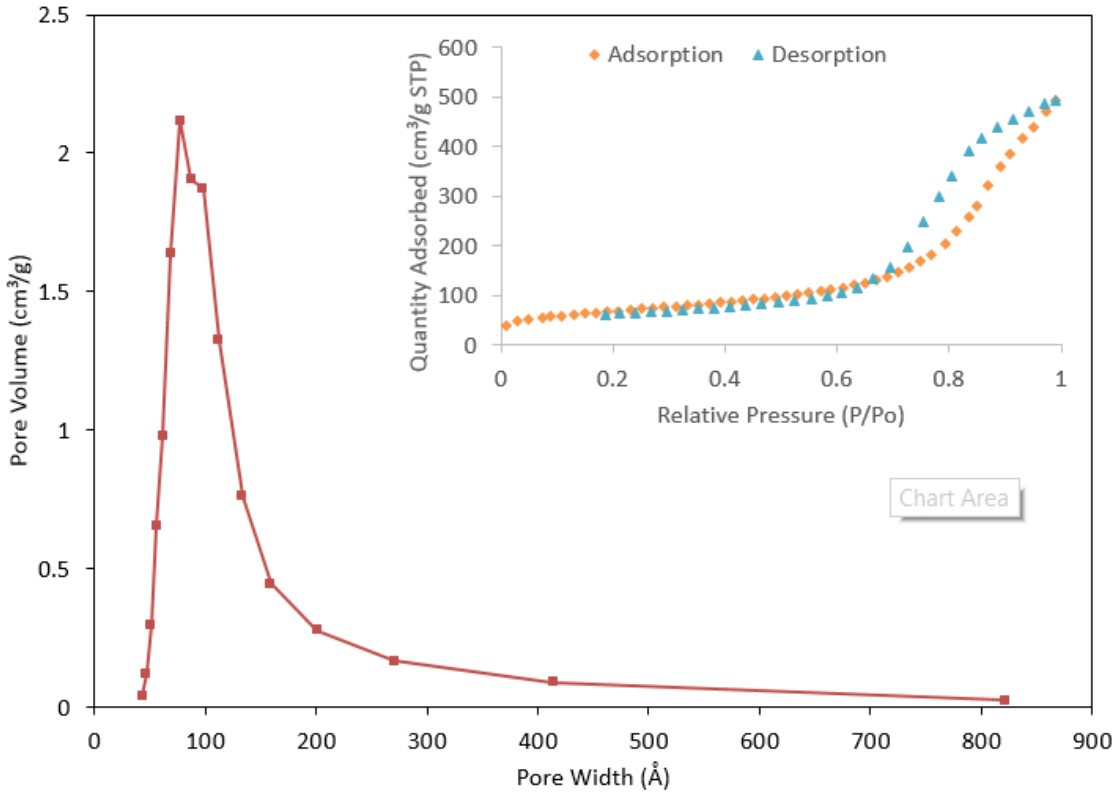

Figure 9. Pore size distribution and nitrogen adsorption isotherm (inset) of the SA 6176 3mm alumina pellets

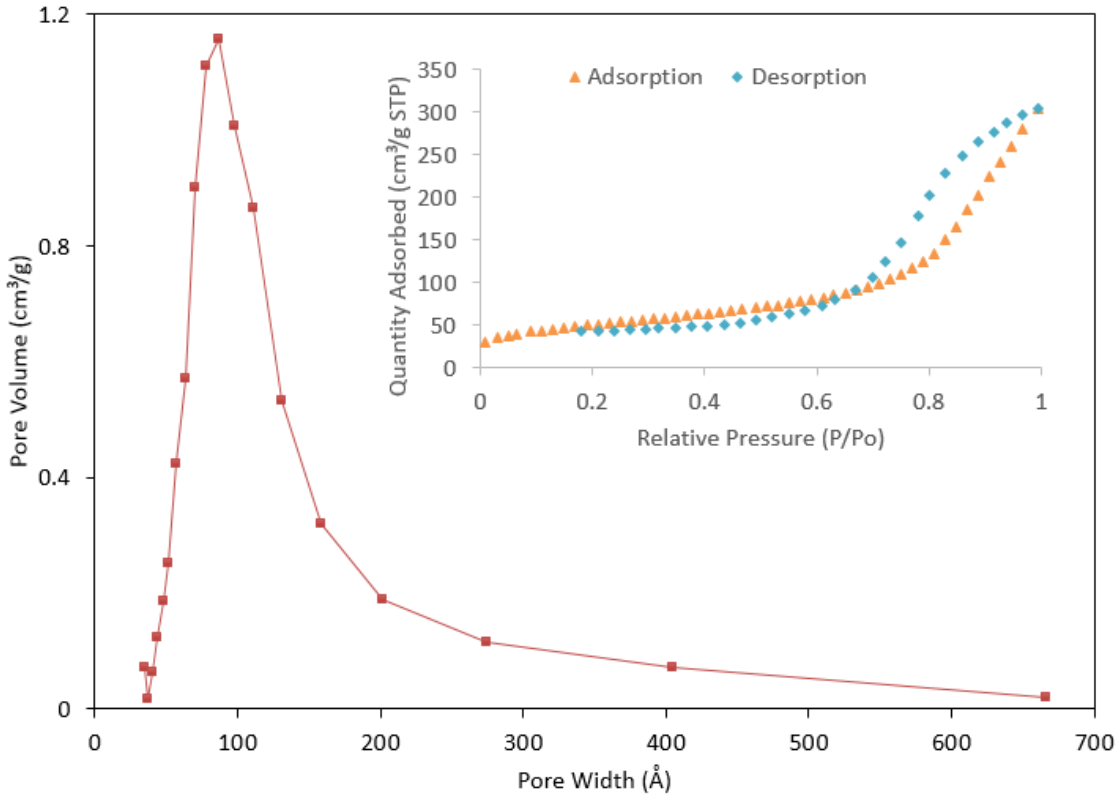

Figure 10. Pore size distribution and nitrogen adsorption isotherm (inset) of alumina pellets after impregnating in 1M $Ni(NO_3)_2$ solution and drying at 100 °C.

2.3.3 Metal Distribution

Figure 11 exhibits the radial metal distribution for samples taken from different positions of the particle bed in the one-heating zone system. As the amount of Ni cannot be obtained instantly from micro-XRF, the ratio between Ni and alumina was calculated to describe the metal distribution. Generally, all the samples have an egg-shell distribution after drying. At the surface of the pellets, the average amount of Ni is around 15 wt%. The ratio drops down to 5 wt% at the core. The parabolic metal distribution curve indicates that the concentration gradient is larger at the surface than in the core. The profiles for the metal distribution in the bottom, middle and top are quite similar. In addition, the difference in metal distribution is not significant between the samples at the wall and at the center.

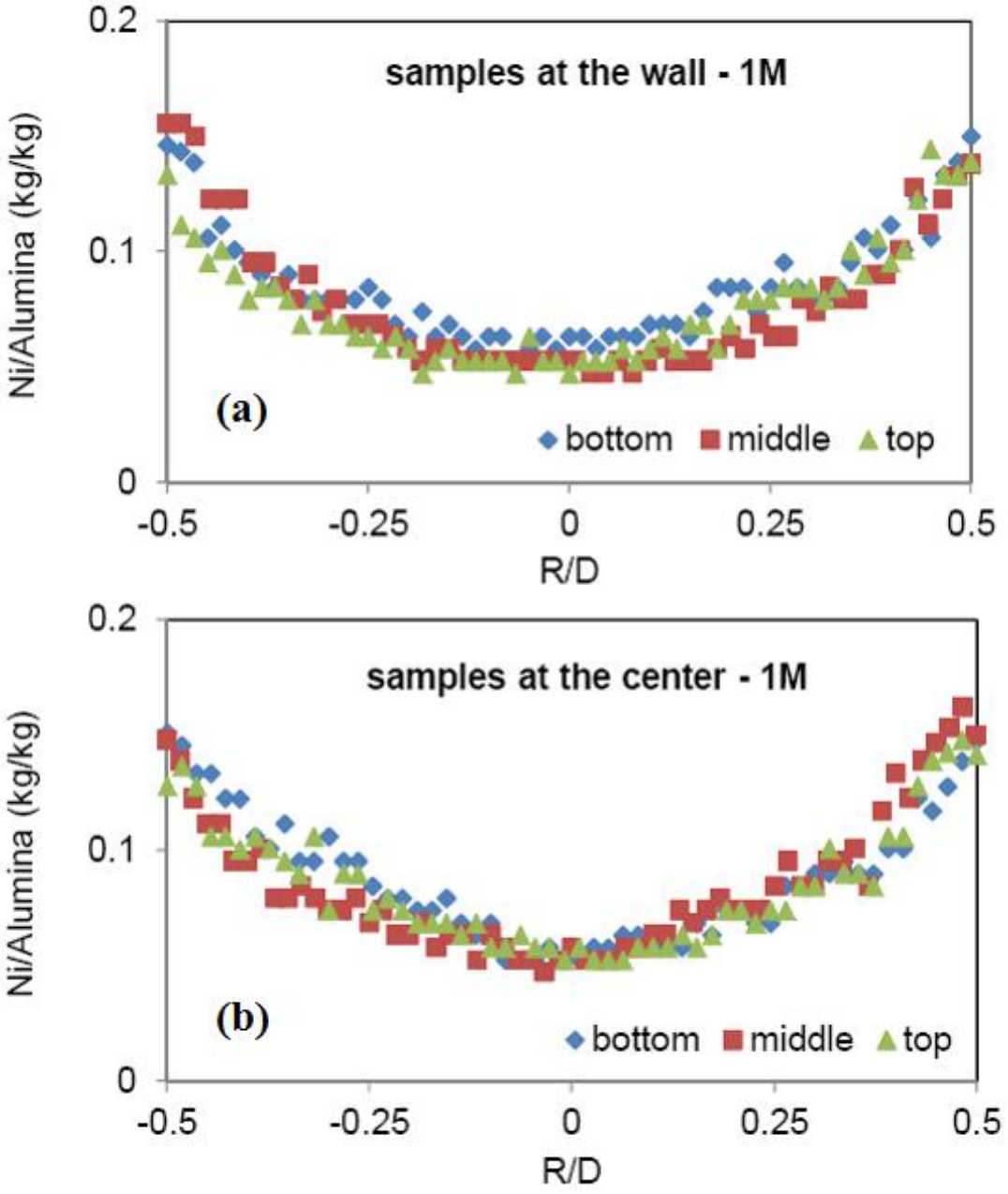

Figure 11. Metal profile after drying at T=100 °C: (a) samples taken at the wall; (b) samples taken at the center (catalysts were impregnated in 1M $Ni(NO_3)_2$ solution)

Some interesting phenomena were observed in the two-heating zone system, where the drying condition varied with time in the particle bed. Different behavior was observed in the high-to-low and the low-to-high temperature pattern. For the high-to-low pattern, as shown in figure 12 (a) and (b), the amount of Ni at the surface and interior of the pellet is

around 13 wt% and 6 wt%, respectively. The profile can be described as a moderate egg-shell distribution. It was a surprise to observe this moderate egg-shell distribution at this operating condition because high temperatures at the first "heating-zone" typically lead to a significant convective flow that will lead to movement of the metal ions outside to the surface leading to a pronounced egg-shell distribution. One possible explanation for not observing the pronounced egg-shell distribution is the effect of melting point depression of the compounds inside the meso-porous structure. Sun et al. reported the confinement induced melting point depression of tin nanoparticles embedded in alumina materials.[26,27] When the size of materials reduces to nano-scale, its melting point tends to drop significantly. The nanoscale compounds are molten and behave like liquid in the pore channels. As a result, the metal ions flow with the molten compounds and redistribute to form a more uniform profile due to the back diffusion.

Figure 12 (c) and (d) show the metal profile for the low-to-high temperature switch pattern. Generally, a pronounced egg-shell distribution was observed. The metal content at the catalysts surface was approximately 25 wt%. The metal content then drops until R/D equals 0.3. At this point, the interior of the pellet maintains a uniform Ni distribution of approximately 6 wt%. Such a metal distribution could be explained by the fact that: (1) the heated air temperature was very low at the first "heating zone", where low convective flow was performed; (2) the heated air temperature increased from 60 °C to above 150 °C in 7 min, which engendered strong convective flow, and therefore metal ion redistribution occurred from the external surface of the pellets and (3) the whole drying process lasted for 25 min. Due to the film breakage effect, which prevents further motion of the dissolved metals from inside to outside, the egg-shell profile stopped at about 30% of the radius from

the surface. At the beginning of the drying process, the liquid phase is continuous throughout the materials. With the proceeding evaporation, breakage of the liquid film throughout the porous structure takes place. The isolated domains in the liquid phase inhibits the liquid flux.[6,7,14] According to Xue et al.[7], at early drying stages, when convective flow dominates, the film breakage effect will cause uniform distribution. If film breakage occurs at late stages of the drying process, egg-shell will be more favorable due to less back diffusion. Once the drying is controlled by the film breakage, when the metal ions are trapped inside the isolated domains, the drying process will no longer change the metal distribution.

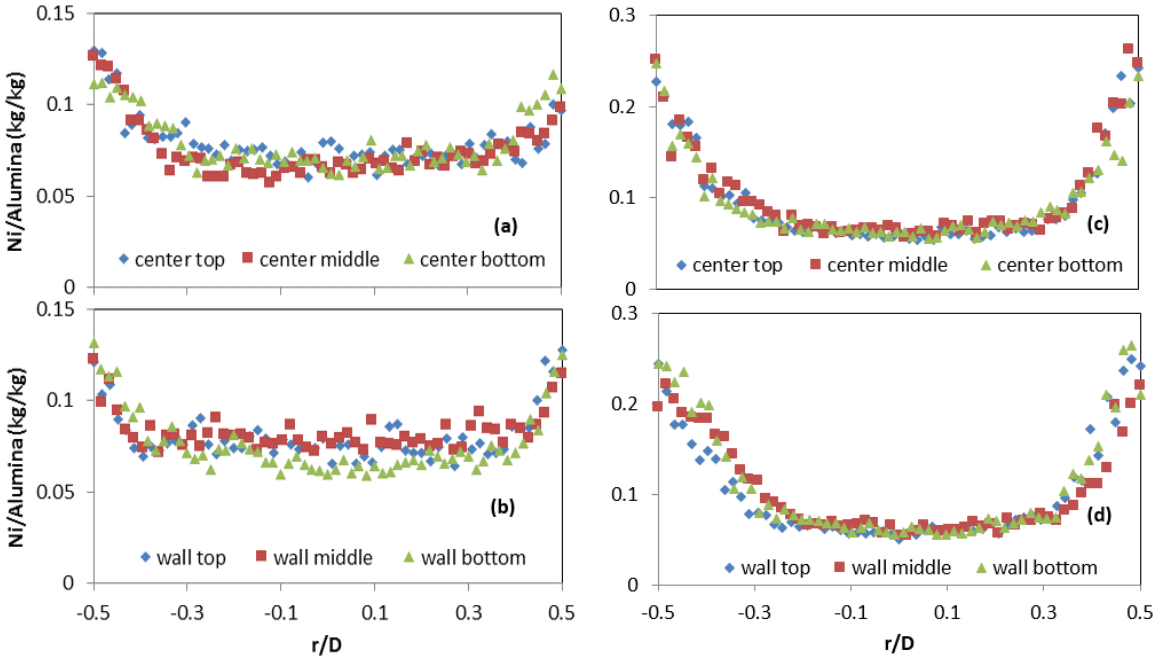

Figure 12. Metal profile: (a) after drying at T_1 = 115 °C then T_2 = 60 °C, samples taken at the center; (b) after drying at T_1 = 115 °C then T_2 = 60 °C, samples taken at the wall; (c) after drying at T_1 = 60 °C then T_2 = 150 °C, samples taken at the center; (d) after drying at T_1 = 60 °C then T_2 = 150 °C, samples taken at the wall. (Catalysts were impregnated in 1M $Ni(NO_3)_2$ solution.)

2.3.4 Melting Point Depression

As was discussed in the previous section, the melting point depression occurs when nickel compounds are reduced to nano-scale within the pore structure. This could be important because if the drying is not enough to eliminate the bound water and the metal compounds are molten even at a low temperature when the solvent evaporates out, the film breakage will be suppressed. If the bound water is removed during drying, causing the melting temperature to become extremely high even when reduced to the nano-scale, the metal ions will be trapped in the isolated domains once the solvent evaporates.

An experiment was designed to test this hypothesis. The alumina pellets were immersed in 3M Ni(NO3)2 solution for 5 days. The first sample was dried in a 60 °C oven to keep the bound water. The second sample was dried in 150 °C oven for 3 hours to make sure all the bound water is eliminated. DSC analysis was performed to study the melting behavior. As shown in the figure 13 (a) and (b), the materials are absorbing energy when heated. Therefore, a peak was expected when the materials starts melting. The peaks are broad because of the different pore sizes inside the materials. In figure 13 (a), an obvious peak is found at 72.56 °C indicating the melting point for nickel nitrate hexahydrate. A change of slope at 42.90 °C reveals a phase transition. The two peaks overlaps since the bulk melting temperature is very close to the depressed melting temperature. In figure 13 (b), there is no peak when heated up to 80 °C because the melting temperature is much higher when all the bound water is gone.

A thermodynamic calculation[28,29] was developed to specify the melting point (T_m):

$$T_m = T_0 \left[1 + \frac{3}{\rho r L_m}(\gamma_{lm} - \gamma_{sm})\right]$$

where T_0 is the bulk melting temperature, ρ is the average density of liquid phase and solid phase, r is the particle radius, L_m is latent heat of melting, Υ_{lm} and Υ_{sm} represent the interfacial energy for liquid-alumina and solid-alumina, respectively. Therefore, the size and the structure of the pores will greatly affect the melting temperature.

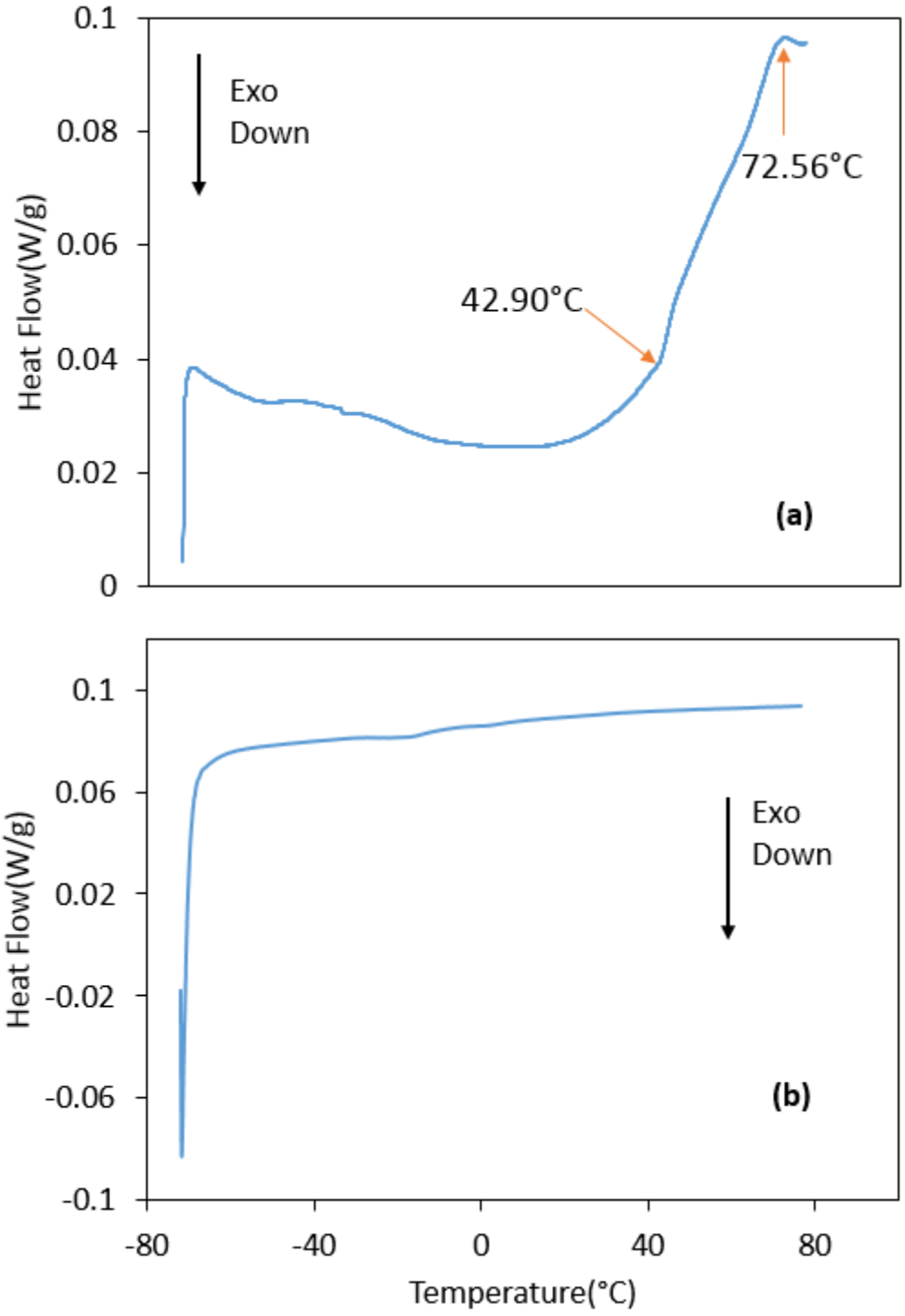

Figure 13. DSC thermograms of the 3 mm alumina pellets impregnated in 3M $Ni(NO_3)_2$ solution after drying in the oven for 3 hours (a) at 60 °C; (b) at 150 °C.

Chapter 3

Conclusions and Future Work

In this thesis, a novel method of investigating the belt drying process was successfully introduced. The packed bed drying was performed in a Glatt GPCG-1 fluidized bed dryer to mimic the drying performance of Ni/Alumina pellets on a belt conveyor. The properties of the catalyst as a function of position on the belt are similar to those as a function of time in the packed bed dryer. For the one-heating zone system, two heating temperatures were adopted, one of which was above and the other below the melting point of the metal precursor. For the two-heating zone system, two drying strategies (i.e. low-to-high and high-to-low patterns) were utilized to investigate the metal profile of the pellets under more sophisticated drying conditions.

In this study, the temperature profile, the surface area, the pore size distribution and the metal distribution of the catalysts were investigated. It was observed that the temperature change was similar in different layers for the single heating zone system. Although a preheating period, which depends on the bed depth, was observed, it didn't make a difference in the resulting metal distribution. In the multi-heating zone system, the temperature delay effect on the upper layers became more significant. Generally, the upper layers followed the same pattern as the bottom layer. However, the top layers failed to reach as high of a temperature due to the delay such that the switch of heating temperature could not be observed in the high-to-low drying pattern.

The pore structure of the catalyst pellets was revealed by BET analysis. Type IV isotherm and a combination of H1 and H4 hysteresis loop type were observed indicating a structure of larger cylindrical pore channels surrounded by slit pores, similar to a tree and its

branches. Therefore, Komiyama's "reservoir" model, in which metal ions are sucked to the external surface by the capillary force through the slit pores, could be utilized to explain the pronounced egg-shell distribution in the one-heating zone system.

The radial metal profile was studied using micro-XRF analysis. A pronounced egg-shell distribution was observed in the one-heating zone system. Moderate egg-shell distributions were found in the two-heating zone system. We found that the effect of film-breakage had a large impact on metal profiles when the layers reached temperatures higher than the melting point of the metal precursor. Thus, the metal profile was curved at the external surface and flat in the core, as discussed in chapter 2. When the temperature of a layer is lower than the melting temperature, film-breakage alone cannot decide the metal profile, and the melting point depression effect should be taken into consideration. The metal ions were thus able to flow inside the porous structure and a flatter distribution was observed in this circumstance.

In this thesis, experiments were conducted with Nickel, a very commonly used metal precursor. Future works on supported catalysts can focus on different metal precursors as well as bimetallic systems. Metals with high melting temperature such as Barium or Molybdenum would be worth studying. Additionally, further simulation work on packed bed drying could help with predicting the drying process, not only in lab scale and pilot scale, but even in manufacturing scale.

Reference

1 Xue Liu, J. G. K., Benjamin J. Glasser. Drying of Supported Catalysts for Low Melting Point Precursors: Impact of Metal Loading and Drying Methods on the Metal Distribution. *Chemical Engineering Science* **79**, 187-199 (2012).

2 Sheng-Yi Lee , R. A. The Distribution of Active Ingredients in Supported Catalysts Prepared by Impregnation. *Catalysis Reviews* **27**, 207 (1985).

3 Azzeddine Lekhal, J. G. K., and Benjamin J. Glasser. Predicting the Effect of Drying on Supported Coimpregnation Catalysts. *Ind. Eng. Chem. Res.* **40**, 3989-3999 (2001).

4 Shyr, Y. S. E., W. Preparation of Nonuniformly Active Catalysts. *J. Catal.* **63**, 425−432 (1980).

5 Gavrilidis, A., Varma, A., Morbidelli, M. Optimal Distribution of catalyst in Pellets. *Catal. Rev.: Sci. Eng.* **35**, 399−456 (1993).

6 A. V. Neimark, L. I. K., and V. B. Fenelonov. Theory of Preparation of Supported Catalysts. *Ind. Eng. Chem. Prod. Res. Dev.* **20**, 439-450 (1981).

7 Xue Liu, J. G. K., Benjamin J. Glasser. Drying of Ni/Alumina Catalysts: Control of the Metal Distribution Using Surfactants and the Melt Infiltration Method. *Industiral & Engineering Chemistry Research* **53**, 5792-5800 (2014).

8 Pinna, F. Supported Metal Catalysts Preparation. *Catalyst Today* **41**, 129-137 (1998).

9 Xue Liu, J. G. K., Benjamin J. Glasser. A Parametric Investigation of Immpregnation and Drying of Supported Catalysts. *Chemical Engineering Science* **63**, 4517-4530 (2008).

10 Khinast, A. L. B. J. G. J. G. Impact of Drying on the Catalyst Profile in Supported Impregnation Catalysts. *Chemical Engineering Science* **56**, 4473-4487 (2001).

11 E.M. Assaf, L. C. J., J.M. Assaf. The Active Phase Distribution in Ni/Al2O3 Catalysts and Mathematical Modeling of the Impregnation Process. *Chemical Engineering Journal* **94**, 93-98 (2003).

12 Kowalski, S. J. Toward a Thermodynamics and Mechanics of Drying Processes. *Chemical Engineering Science* **55**, 1289-1304 (2000).

13 Waananena, K. M., Litchfieldb,J.B.,Okos,M.R. Classification of Drying Models for Porous Solids. *Drying Technology* **11**, 1-40 (1993).

14 A. V. Neimark, V. B. F., L. I. Kheifets. Analysis of the Drying Stage in theTechnology of Supported Catalysts. *Reacr. Kinet. Catal. Lett.* **5**, 67-72 (1976).

15 Masaharu Komiyam, R. P. M., H. F. Harnsberger. Concentration Profiles in Impregnation of Porous Catalysts: Nickel on Alumina. *Journal of Catalysis* **63**, 35-52 (1980).

16 Yoshimitsu Uemura, Y. H., Atsushi Ikari. Formation of Nickel Concentration Profile in Nickel/Alumina Catalyst During Post-impregnation. *Journal of Chemical Engineering of Japan* **6**, 117-123 (1973).

17 Azzeddine Lekhal, B. J. G., Johannes G. Khinast. Influence of pH and Ionic Strength on the Metal Profile of Impregnation Catalysts. *Chemical Engineering Science* **59**, 1063-1077 (2004).

18 Xue Liu, J. G. K., Benjamin J. Glasser. in *2014 American Institude of Chemical Engineers Annual Meeting.*

19 E. F. Zanoelo, A. A., L.A.C. Meleiro. Dynamic Modeling and Feedback Control for Conveyors-Belt dryers of Mate Leaves. *Journal of Food Engineering* **84**, 458-468 (2007).

20 Katrin Burmester, A. P., Rudolf Eggers. A Basic Investigation on Instant Coffee Production by Vacuum Belt Drying *Procedia Food Science 1* **2011**, 1344-1352 (2011).

21 Xue Liu, J. G. K., Benjamin J. Glasser. Drying of Supported Catalysts: A Comparison of Model Predictions and Experimental Measurements of Metal Profiles. *Ind. Eng. Chem. Prod. Res.* **49**, 2649-2657 (2010).

22 Tamara M. Eggenhuisen, J. P. d. B., Dirkjan Verdoes, Petra E. de Jongh, and Krijn P. de Jong. Fundamentals of Melt Infiltration for the Preparation of Supported Metal Catalysts. The Case of Co/SiO2 for Fischer-Tropsch Synthesis. *Journal of the American Chemical Society* **132**, 18318-18325 (2010).

23 Sandeep Badoga, R. V. S., Ajay K. Dalai, John Adjaye. Synthesis and characterization of mesoporous aluminas with different pore sizes: Application in NiMo supported catalyst for hydrotreating of heavy gas oil. *Applied Catalysis A: General* **489**, 86-97 (2015).

24 Dilek Angın, E. A., Tijen Ennil Köse. Influence of process parameters on the surface and chemical properties of activated carbon obtained from biochar by chemical activation. *Bioresource Technology* **148**, 542-549 (2013).

25 Qian Wang, J. Y., Yanbo Wang, Tong Wei, Milin Zhang, Xiaoyan Jing, Zhuangjun Fan. Three-dimensional flower-like and hierarchical porous carbon materials as high-rate performance electrodes for supercapacitors. *Carbon* **67** (2014).

26 Pei-Ling Sun , S.-P. W., Tsung-Shune Chin. Melting Point Depression of Tin Nanoparticles Embedded in a Stable Alpha-Alumina Matrix Fabricated by Ball Milling. *Materials Letters* **144**, 142-145 (2015).

27 Pei-Ling Sun , S.-P., Shih-ChinChang , Tsung-ShuneChin , Rong-TanHuang. Micro Structure and Melting Behavior of Tin Nanoparticles Embedded in Alumina Matrix Processed by Ball Milling. *Materials Science and Engineering A* **600**, 59-66 (2014).

28 H. W. SHENG, K. L., E. MA. Melting and Freezing Behavior of Embedded Nanoparticles in Ball-Milled Al–10 wt% M (M=In, Sn, Bi, Cd, Pb) Mixtures. *Acta Materialia* **46**, 5195-5205 (1998).

29 G.L. Allen, W. W. G., W.A. Jesser. The Melting Temperature of Microcrystals Embedded in a Matrix. *Acta Metallurgica* **28**, 1695-1701 (1980).